

# Composition evolution of nanoscale Al<sub>3</sub>Sc precipitates in an Al–Mg–Sc alloy: Experiments and computations

Emmanuelle A. Marquis<sup>a,b</sup>, David N. Seidman<sup>b,\*</sup>, Mark Asta<sup>b</sup>, Christopher Woodward<sup>b,c</sup>

<sup>a</sup> Materials Physics Department, Sandia National Laboratories, 7011 East Avenue, MS 9161, Livermore, CA 94550, United States

<sup>b</sup> Materials Science and Engineering Department, Northwestern University, Evanston, IL 60208-3108, United States

<sup>c</sup> Materials and Manufacturing Directorate, Air Force Research Laboratory, Wright Patterson AFB, OH 45433, United States

Received 7 May 2005; received in revised form 18 August 2005; accepted 22 August 2005

Available online 25 October 2005

## Abstract

Controlling the distribution of chemical constituents within complex, structurally heterogeneous systems represents one of the fundamental challenges of alloy design. We demonstrate how the combination of recent developments in sophisticated experimental high resolution characterization techniques and ab initio theoretical methods provide the basis for a detailed level of understanding of the microscopic factors governing compositional distributions in metallic alloys. In a study of the partitioning of Mg in two-phase ternary Al–Sc–Mg alloys by atom-probe tomography, we identify a large Mg concentration enhancement at the coherent  $\alpha$ -Al/Al<sub>3</sub>Sc heterophase interface with a relative Gibbsian interfacial excess of Mg with respect to Al and Sc,  $\Gamma_{\text{Mg}}^{\text{rel}}$ , equal to  $1.9 \pm 0.5$  atom nm<sup>-2</sup>. The corresponding calculated value of  $\Gamma_{\text{Mg}}^{\text{rel}}$  is  $\sim 1.2$  atom nm<sup>-2</sup>. Theoretical ab initio investigations establish an equilibrium driving force for Mg interfacial segregation that is primarily chemical in nature and reflects the strength of the Mg–Sc interactions in an Al-rich alloy.

© 2005 Acta Materialia Inc. Published by Elsevier Ltd. All rights reserved.

**Keywords:** Atom-probe tomography; Ab initio calculations; Al<sub>3</sub>Sc precipitates; Mg segregation; Coherent heterophase interface

## 1. Introduction

With continuing rapid increases in computing power, computational modeling is increasingly augmenting traditional empirical investigations in the design of technologically advanced structural materials. Most high-performance metallic alloys contain multiple alloying elements, whose interactions govern the formation of strengthening second-phases, partitioning behavior, and segregation at internal interfaces such as grain boundaries or matrix/precipitate heterophase interfaces. Since such compositional variations are a critical factor governing the mechanical properties, theoretical understanding of interatomic interactions in multicomponent alloys is highly desirable from the standpoint of designing such materials.

In the case of Al alloys, scandium contributes significantly to improving strength by forming nanoscale coherent Al<sub>3</sub>Sc precipitates [1,2]. Additions of ternary elements aim at improving mechanical properties and nanostructural stability. Transition metals, such as Ti and Zr tend to decrease the coarsening kinetics of the L1<sub>2</sub> phase [3,4] whereas Mg resides exclusively in the  $\alpha$ -Al matrix in solid solution [1]. This paper focuses on the effects of Mg additions on Al<sub>3</sub>Sc precipitation in Al–Sc alloys, which is important for optimizing the mechanical properties of these multicomponent alloys [5], and is part of a comprehensive study of the room temperature and elevated temperature (573 K) creep behavior of Al(Sc) based alloys [3–10]. From a fundamental viewpoint, addition of Mg to the  $\alpha$ -Al/Al<sub>3</sub>Sc system, where Mg is an oversized atom (12.08% by radius and 40.82 by volume [11]) in solid solution in the  $\alpha$ -Al matrix, constitutes a simple and well-defined system for studying elemental partitioning and heterophase segregation. This research builds on our initial

\* Corresponding author. Tel.: +1 8474914391/9252943287.

E-mail addresses: [d-seidman@northwestern.edu](mailto:d-seidman@northwestern.edu), [emarqui@sandia.gov](mailto:emarqui@sandia.gov) (D.N. Seidman).

results obtained by high-resolution electron microscopy (HREM), showing that Mg additions alter the morphology of  $\text{Al}_3\text{Sc}$  precipitates, that is, the  $\{100\}$  and  $\{110\}$  facets disappear and the precipitates become spheroidal [6,7]. Asta et al. recently published first-principles calculations demonstrating significant Mg segregation at coherent  $\{100\}$   $\alpha\text{-Al}/\text{Al}_3\text{Sc}$  coherent interfaces [12,13]. The present study demonstrates how the behavior of Mg in  $\alpha\text{-Al}/\text{Al}_3\text{Sc}$  alloys can be both measured at the subnanoscale level using atom-probe tomography (APT) and predicted from ab initio calculations, thereby providing detailed insight into the driving forces for phase partitioning and interfacial segregation in this model two-phase ternary aluminum alloy.

## 2. Experimental procedures

### 2.1. Specimen preparations

A cast Al alloy with nominal composition 2.2 Mg–0.12 at.% Sc was annealed at 618 °C in air for 24 h (to ensure uniformity of the Mg concentration throughout the material), quenched into cold water, and then aged in air at 300 °C for times between 0.33 and 1040 h.

APT tips were obtained by a two-step electropolishing procedure. The initial polishing solution of 30 vol.% nitric acid in methanol was followed by a solution of 2 vol.% perchloric acid in butoxyethanol, used for final polishing to produce a sharply pointed tip, with a radius of curvature of less than 100 nm (Fig. 1). Field-ion microscopy (FIM) analyses were performed at a background pressure of  $10^{-5}$  Torr consisting of a mixture of 80% Ne and 20% He; APT analyses were carried out under ultrahigh vacuum conditions ( $10^{-10}$  Torr) for pulsed field-evaporation, which was performed with a pulse fraction (pulse voltage/steady state dc voltage) of 20% and a pulse frequency of 1500 Hz. Specimens were maintained at temperatures below 30 K.

After aging for 0.5 h at 300 °C, the precipitate number density,  $4 \pm 2 \times 10^{22}$  precipitate  $\text{m}^{-3}$  [8], is sufficiently high to perform APT random-area analysis. The error bars stated correspond to one standard deviation. After aging for 1040 h at 300 °C, the number density of  $\text{Al}_3\text{Sc}$  precipitates decreases to about  $3 \pm 1 \times 10^{21}$  precipitate  $\text{m}^{-3}$ , and random area APT analysis is no longer an efficient technique. Hence, FIM imaging was first performed to locate precipitates that are just commencing to intersect the surface of a tip before starting an analysis.

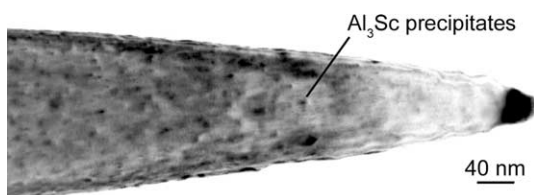


Fig. 1. Transmission electron micrograph of an APT tip, illustrating the coherency strain contrast of the  $\text{Al}_3\text{Sc}$  precipitates after aging at 300 °C for 5 h.

### 2.2. Data analysis

A typical mass-to-charge state ( $m/n$ ) spectrum is displayed in Fig. 2. The three isotopes of Mg are doubly charged at 12, 12.5 and 13 a.m.u., with no hydride formation. The measured isotopic abundances are  $78.4 \pm 0.3\%$  for  $^{24}\text{Mg}^{2+}$ ,  $10.5 \pm 0.3\%$  for  $^{25}\text{Mg}^{2+}$  and  $11.1 \pm 0.3\%$  for  $^{26}\text{Mg}^{2+}$ , which agree favorably with the handbook values of 79%, 10% and 11%. Scandium is also doubly charged with multiple hydrides, exhibiting a possible overlap between Sc and singly charged Mg at  $m/n$  values of 24, 25 and 26 a.m.u. In some cases, peaks at 24, 25 or 26 a.m.u. are detected, but the correct mass ratio of the isotope  $^{24}\text{Mg}$  to the other two isotopes,  $^{25}\text{Mg}$ , and  $^{26}\text{Mg}$ , was not found; therefore the corresponding ions were considered to be Sc hydrides. Since one of the objectives of this study is the measurement of Mg concentrations, this choice implies possibly under-estimating the Mg concentrations, in particular in the proximity of the  $\text{Al}_3\text{Sc}$  precipitates.

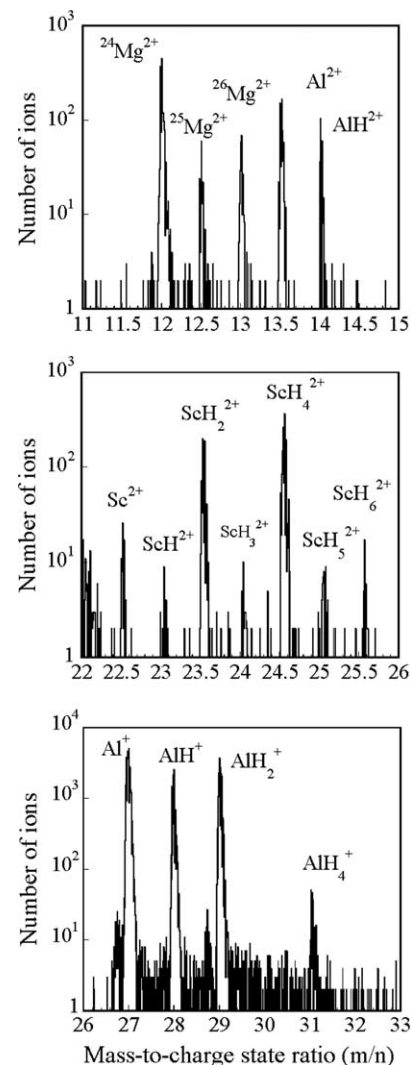


Fig. 2. Example of mass-to-charge state ratio ( $m/n$ ) spectra from a tip containing an  $\text{Al}_3\text{Sc}$  precipitate.

Data visualization and analysis of data sets were performed using a software code, ADAM 1.5, which was developed at Northwestern specifically for analyzing APT data [14].

### 3. Results

In the as-quenched state, Mg and Sc appear homogeneously distributed although the standard statistical  $\chi^2$ -test used [15], which compares solute concentration distributions with binomial distributions of a perfectly random solid solution, does not rule out whether or not Mg or Sc atoms are homogeneously distributed in the  $\alpha$ -Al matrix.

Precipitates are observed after aging for 0.33 h (Fig. 3(a)). A cluster search algorithm with a maximum separation distance of 0.7 nm is used to isolate the Sc atoms constituting the precipitates. Taking into account the spherical morphology of the precipitates [8], the composition was measured in spherical shells centered on the center-of-mass of the selected Sc atoms. Eight precipitates were analyzed yielding an average concentration of  $22.4 \pm 2.8$  at.% Sc. The radius of these  $\text{Al}_3\text{Sc}$  precipitates, estimated using the radius of gyration of the Sc atoms, is

between 0.8 and 1.4 nm. Magnesium atoms are also present inside the precipitates at a level, 4.3 at.%, which is approximately a factor of two greater than the average Mg concentration in the  $\alpha$ -Al matrix.

After further aging, the precipitate radius increases (Figs. 3(b) and (c)) and reaches about 4 nm at 1040 h (Fig. 4). The spatial resolution of APT is illustrated in Fig. 4, where an analysis performed near the 110 crystallographic pole reveals the {220} atomic planes perpendicular to the analysis direction. The Sc concentration of the precipitates increases after 0.5 h and remains constant thereafter within experimental error,  $x_{\text{Sc}} = 27.4 \pm 1.5$  at.% Sc (Table 1). The small discrepancy with the nominal composition, i.e. 25 at.%, is likely to be due to the different evaporation fields of Al and Sc that could not be accommodated despite the low tip temperature <30 K. On the other hand, the Mg concentration decreases with increasing aging time to 0.9 at.% after 1040 h aging. The Mg concentration within the  $\text{Al}_3\text{Sc}$  precipitates is non-uniform with an enhancement at their centers as shown in the example of Fig. 5.

For aging times longer than 2 h, a distinct Mg concentration enhancement at the  $\alpha$ -Al/ $\text{Al}_3\text{Sc}$  heterophase interface is also observed. The example displayed in Fig. 5 is a proximity histogram [16] that calculates the average composition in shells of 0.4 nm thickness at a given distance from the  $\alpha$ -Al/ $\text{Al}_3\text{Sc}$  heterophase interface. The interface is defined by an isoconcentration surface at 18 at.% Sc. The Mg concentration enhancement at the  $\alpha$ -Al/ $\text{Al}_3\text{Sc}$  heterophase interface is 200%, which is localized within 2 nm at this heterophase interface. The maximum Mg concentration at this heterophase interface decreases slightly during the early aging times and thereafter remains constant within experimental error. Fig. 6 displays the normalized average Mg concentration profile taken from the centers of the precipitates for each aging time. The profiles are temporally invariant after 2 h.

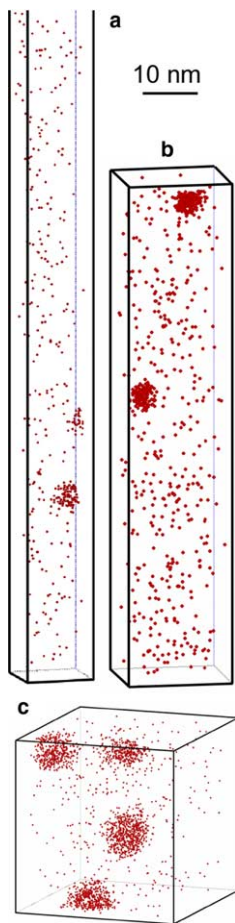


Fig. 3. Three-dimensional reconstruction of an analyzed volume, displaying only the Sc atoms, from a specimen aged at 300 °C for: (a) 0.33 h; (b) 0.5 h; and (c) 5 h.

## 4. Discussion

### 4.1. Mg segregation: experimental measurement

Mg segregation at the  $\alpha$ -Al/ $\text{Al}_3\text{Sc}$  interface is constant with aging time, which suggests that the measured concentrations represent an equilibrium behavior. Moreover, the root-mean-square diffusion distance of Mg in Al is given by  $\sqrt{6Dt}$ , where the factor 6 is for diffusion in 3-dimensions;  $D = 1.6 \times 10^{-16} \text{ m}^2 \text{ s}^{-1}$  is the diffusion coefficient of Mg in Al [17] at 300 °C and  $t$  is the aging time; the values are about 1.3  $\mu\text{m}$  after 0.5 h aging at 300 °C and 60  $\mu\text{m}$  after 1040 h. The precipitate spacing is evaluated using the square-lattice spacing approximation, which is given by  $\langle R \rangle = \sqrt[3]{4\pi/3f}$ , where  $\langle R \rangle$  is the mean precipitate radius and  $f = 0.53$  vol.% is the calculated volume fraction of  $\text{Al}_3\text{Sc}$  precipitates at 300 °C. The precipitate spacing is 10 nm for  $\langle R \rangle$  equal to 1.1 nm (0.5 h aging), and 39 nm for  $\langle R \rangle$  equal to 4.2 nm (1040 h aging). The root-mean-square

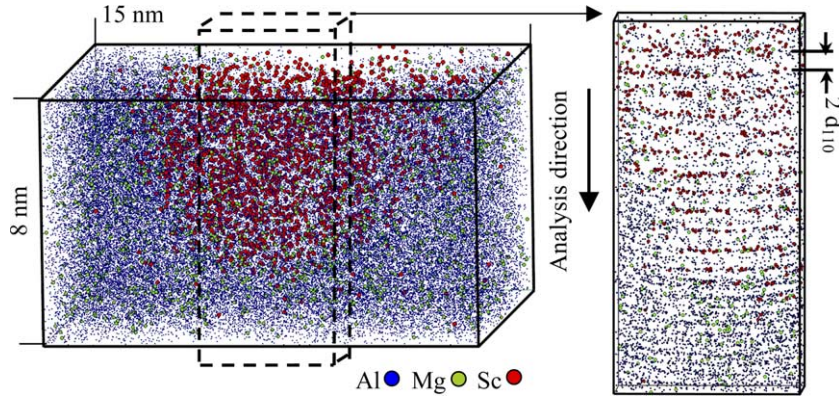


Fig. 4. Three-dimensional reconstruction of an  $\text{Al}_3\text{Sc}$  precipitate after aging at  $300^\circ\text{C}$  for 1040 h; Al atoms are in blue, Mg atoms in green and Sc atoms in red.

Table 1  
 $\text{Al}_3\text{Sc}$  precipitate composition as function of aging time at  $300^\circ\text{C}$

Time (h)	Number of precipitates	Al (at.%)	Mg (at.%)	Sc (at.%)
As quenched	0	–	–	–
0.33	8	$73.3 \pm 3.5$	$4.3 \pm 2.6$	$22.4 \pm 2.8$
0.5	4	$68.8 \pm 5.2$	$4.09 \pm 1.5$	$28.5 \pm 1.4$
2	10	$71.2 \pm 1.4$	$2.3 \pm 0.6$	$26.5 \pm 1.4$
5	3	$68.9 \pm 2.1$	$3.1 \pm 1.1$	$28.1 \pm 2.5$
30	2	$71.0 \pm 2.8$	$2.5 \pm 0.8$	$26.5 \pm 2.3$
1040	15	$69.4 \pm 2.8$	$0.9 \pm 0.3$	$29.2 \pm 2.4$

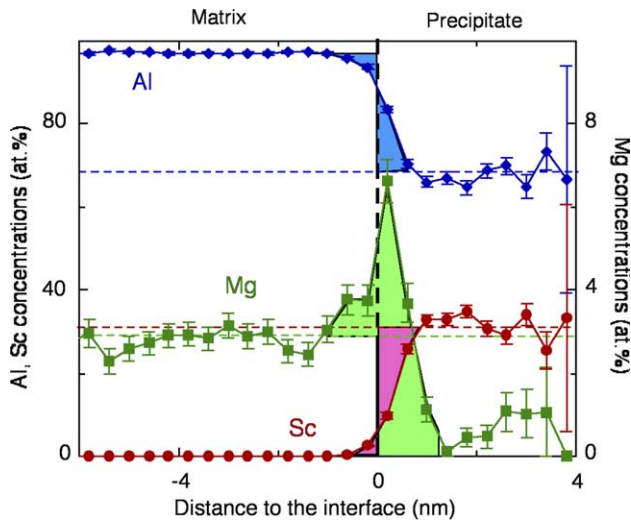


Fig. 5. Proximity histogram of an  $\text{Al}_3\text{Sc}$  precipitate after aging at  $300^\circ\text{C}$  for 1040 h; the colored areas correspond to the interfacial excesses of Al (blue), Mg (green) and Sc (red).

diffusion distance of Mg is therefore always significantly greater than the average center-to-center precipitate spacing and the system is at the very least in local thermodynamic equilibrium with respect to Mg segregation at the  $\alpha\text{-Al}/\text{Al}_3\text{Sc}$  heterophase interface.

The relative Gibbsian interfacial excess concentration of Mg with respect to Al and Sc provides a quantitative thermodynamic description of the observed equilibrium Mg segregation, and it is given by [18]:

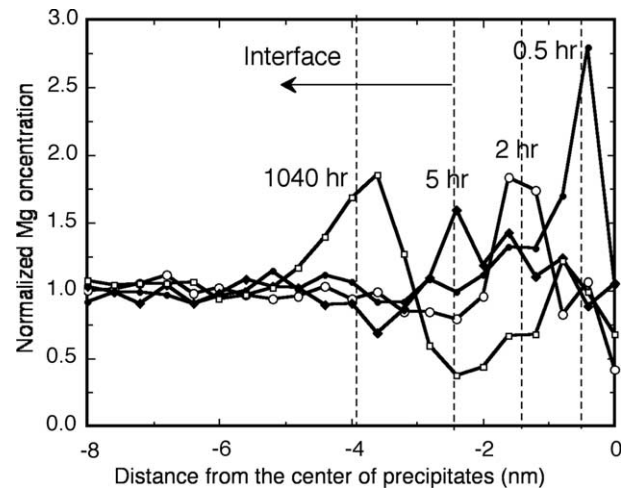


Fig. 6. Mg concentration normalized by the average Mg concentration in the  $\alpha\text{-Al}$  matrix for four different aging times (0.5, 2, 5, and 1040 h) at  $300^\circ\text{C}$ .

$$\Gamma_{\text{Mg}}^{\text{rel}} = \Gamma_{\text{Mg}} - \Gamma_{\text{Sc}} \frac{x_{\text{Al}}^{\alpha} x_{\text{Mg}}^{\alpha'} - x_{\text{Al}}^{\alpha'} x_{\text{Mg}}^{\alpha}}{x_{\text{Al}}^{\alpha} x_{\text{Sc}}^{\alpha'} - x_{\text{Al}}^{\alpha'} x_{\text{Sc}}^{\alpha}} - \Gamma_{\text{Al}} \frac{x_{\text{Mg}}^{\alpha} x_{\text{Sc}}^{\alpha'} - x_{\text{Mg}}^{\alpha'} x_{\text{Sc}}^{\alpha}}{x_{\text{Al}}^{\alpha} x_{\text{Sc}}^{\alpha'} - x_{\text{Al}}^{\alpha'} x_{\text{Sc}}^{\alpha}}, \quad (1)$$

where  $\Gamma_{\text{Mg}}$ ,  $\Gamma_{\text{Sc}}$  and  $\Gamma_{\text{Al}}$  are the Gibbsian interfacial excesses of Mg, Sc, and Al, respectively, and the  $x_j^{\alpha}$  and  $x_j^{\alpha'}$  are the concentrations of component  $j$  ( $j = \text{Al}$ , Sc or Mg) in phase  $\alpha$  (Al) and  $\alpha'$  ( $\text{Al}_3\text{Sc}$ ). Fig. 5 displays the Gibbsian excess quantities for Al (negative value), Mg and Sc (positive values) as areas under the concentration curves in the proximity histogram [19]. The relative Gibbsian excesses of Mg with respect to Al and Sc are listed in Table 2 for the different aging times. The variations observed are within the experimental errors. The similar values of the Gibbsian excess of Mg relative to Al and Sc for all aging times implies that the system is at the very least in local thermodynamic equilibrium and the average value is  $\Gamma_{\text{Mg}}^{\text{rel}} = 1.9 \pm 0.5 \text{ atom nm}^{-2}$ . For the Al–Sc–Mg system, the calculations of the solute concentrations at the interface of a growing  $\text{Al}_3\text{Sc}$  precipitate predict a depletion of Mg at

Table 2

Precipitate radius (from [7]), relative Gibbsian interfacial excess of Mg as function of aging time at 300 °C, and maximum Mg enhancement factor

Aging time (h)	0.5	2	5	30	1040
Radius (nm)	1	–	2	–	4.2
$\Gamma_{\text{Mg}}^{\text{rel}}$ <sup>a</sup>	$1.5 \pm 0.7$	$1.7 \pm 0.4$	$1.7 \pm 0.3$	$2.22 \pm 0.45$	$1.85 \pm 0.38$
$c_{\text{Mg}}^{\text{max}}/c_{\text{Mg}}^{\text{matrix}}$	$2.8 \pm 0.3$	$2.7 \pm 0.2$	$2.0 \pm 0.2$	$2.3 \pm 0.5$	$1.9 \pm 0.5$

<sup>a</sup> Calculated using Eq. (1).

the  $\alpha$ -Al/Al<sub>3</sub>Sc interface (see below and Table 3). Thus our observation of a positive value of the relative Gibbsian interfacial excess of Mg with respect to Al and Sc is further evidence that we are observing a true thermodynamic equilibrium excess quantity.

The decrease in interfacial free energy associated with Mg segregation can be estimated using [20]:

$$\Gamma_{\text{Mg}}^{\text{rel}} = - \left( \frac{\partial \gamma}{\partial \mu_{\text{Mg}}} \right)_{\text{T,P}}, \quad (2)$$

where  $\Gamma_{\text{Mg}}^{\text{rel}}$  is the relative Gibbsian excess of Mg with respect to Al and Sc, and  $\mu_{\text{Mg}}$  is the chemical potential of Mg. Assuming an ideal solid-solution, the chemical potential is  $\mu_{\text{Mg}} = \mu_0 + k_{\text{B}}T \ln(x_{\text{Mg}}^{\alpha})$ , and it yields the following expression:

$$\left( \frac{\partial \gamma}{\partial x_{\text{Mg}}} \right)_{\text{T,P}} = - \frac{\Gamma_{\text{Mg}}^{\text{rel}} k_{\text{B}}T}{x_{\text{Mg}}^{\alpha}}. \quad (3)$$

At 300 °C, the measured relative Gibbsian excess of Mg with respect to Al and Sc is  $\Gamma_{\text{Mg}}^{\text{rel}} = 1.9 \pm 0.5 \text{ atom nm}^{-2}$ , and the average Mg concentration in the matrix is  $x_{\text{Mg}}^{\alpha} = 2.2 \pm 0.3 \text{ at.}\%$  Mg. Assuming  $\Gamma_{\text{Mg}}^{\text{rel}}$  varies linearly with concentration, the integration of Eq. (3) for  $x_{\text{Mg}}^{\alpha}$  varying from 0 to 0.022 yields a decrease in the interfacial free energy of  $15 \text{ mJ m}^{-2}$ .

Several previous APT studies reported segregation behavior of solute atoms at partially semi-coherent or semi-coherent heterophase interfaces [22,23]. In the present study, the coherency state of the  $\alpha$ -Al/Al<sub>3</sub>Sc interface is known from HREM observations, and was determined to be perfectly coherent for all cases presented. Coherency loss may occur when the precipitate diameter is sufficiently large. For the lattice parameter misfit at 300 °C,  $\delta \approx 0.62\%$ , between the Al matrix containing 2.2 at.% Mg and the Al<sub>3</sub>Sc phase, the spacing between the misfit dislocations is  $a/\delta$ , where  $a \approx 0.2 \text{ nm}$  is the spacing between {200}

planes; this yields a critical precipitate diameter for loss of coherency of approximately 30 nm, which is much greater than the precipitate diameter measured after aging at 300 °C for less than 1040 h.

The exact shape of the precipitates observed by APT needs to be carefully considered. Firstly, the observations may be subject to experimental artifacts, such as asymmetry of the tip, or misalignment of the analysis direction. Also, the results depend strongly on the field evaporation behaviors of the  $\alpha$ -Al matrix and Al<sub>3</sub>Sc precipitates, which may be significantly different. The measured local atomic density of the  $\alpha$ -Al matrix is indeed higher than that of the precipitate phase, with an experimental density ratio equal to about 1.4. It is consistent with the bright imaging of the Al<sub>3</sub>Sc precipitates in FIM mode, indicating that the precipitates exhibit a small protrusion effect, due to their higher evaporation field. The width of the heterophase interface may therefore be explained by the artificially higher magnification of the Al<sub>3</sub>Sc precipitates and possibly ion trajectory effects [24]. The approximately spheroidal shape of the Al<sub>3</sub>Sc precipitates observed by HREM is, however, reproduced and no significant distortions between the lateral dimension and the depth dimension are observed.

#### 4.2. Driving force for Mg segregation

In this section we employ first-principles calculations to analyze the microscopic factors governing the pronounced enhancement of Mg at the Al/Al<sub>3</sub>Sc interface. In this analysis we first make use of the theoretical framework provided by a model of diffusion-limited precipitate growth kinetics, to ascertain whether the measured Mg enhancement may be due simply to capillary effects. The analysis leads to the conclusion that the Mg enhancement measured by APT cannot be interpreted simply as reflecting the effects of capillarity and solute-flux balance in a model of diffusion-limited growth. We subsequently use first-principles calculations to establish that the interfacial enhancement corresponds to an equilibrium segregation phenomenon driven by a chemical driving force reflecting the attractive interactions between Mg and Sc solute atoms.

##### 4.2.1. Interface solute concentrations in a model of diffusion-limited growth

In this section we explore whether the solute-concentration profiles measured by APT can be interpreted as representing steady-state solutions to the solute diffusion equation, subject to the boundary conditions imposed by

Table 3

Values of solute concentrations at the precipitate/matrix interface calculated from Eqs. (4) and (5) for spherical  $\alpha'$  (Al<sub>3</sub>Sc) precipitates of radius  $R$  growing in a supersaturated  $\alpha$  (Al) matrix in a ternary Al–Sc–Mg alloy

$R$ (nm)	$\hat{x}_{\text{Sc}}^{\alpha}$ (at. %)	$\hat{x}_{\text{Mg}}^{\alpha}$ (at. %)	$\hat{x}_{\text{Sc}}^{\alpha'}$ (at. %)	$\hat{x}_{\text{Mg}}^{\alpha'}$ (at. %)
2	$2.5 \times 10^{-4}$	2.2	25	$3.4 \times 10^{-7}$
4	$1.8 \times 10^{-4}$	2.2	25	$4.0 \times 10^{-7}$
$\infty$	$9.0 \times 10^{-5}$	2.4	25	$4.8 \times 10^{-7}$

These values were derived assuming values for the interfacial free energy,  $\sigma$  equal to  $0.175 \text{ J m}^{-2}$  [21] that are independent of composition and radius, as discussed in the text.

local thermodynamic equilibrium and flux balance at the growing precipitate/matrix interface. In this analysis we employ a model for diffusion-limited growth of precipitates in a ternary alloy due to Kuehmann and Voorhees [25]. While in a binary alloy the condition of local thermodynamic equilibrium uniquely determines the interfacial solute compositions at the interface during diffusion-limited growth, the situation is qualitatively different in a ternary alloy. As described in [25], the conditions of local thermodynamic equilibrium provide only three equations (equality of chemical potentials for each of the chemical species), which do not determine uniquely the four independent values of the interface solute concentrations (two in each of the two phases). Within a diffusion-limited-growth model for a ternary alloy, the additional constraint required to fix the interface compositions arises from the requirement of mass conservation (flux balance) at the moving precipitate/matrix interface. As a consequence, interface compositions in a ternary alloy are dictated not only by bulk and interfacial thermodynamic properties, but also by the ratio of the diffusivities in the matrix phase, which affect the relative fluxes of each solute species.

For spherical precipitate geometries, employing a mean-field, quasi-steady-state solution to the diffusion equation (neglecting off-diagonal terms in the diffusion matrix), interface compositions can be derived from the following equations [25]:

$$\mu_i^\alpha(\hat{x}_{\text{Mg}}^\alpha, \hat{x}_{\text{Sc}}^\alpha) - \mu_i^{\alpha'}(\hat{x}_{\text{Mg}}^{\alpha'}, \hat{x}_{\text{Sc}}^{\alpha'}) = \frac{2\gamma}{R} \bar{V}_i (i = \text{Al}, \text{Sc}, \text{Mg}), \quad (4)$$

$$\frac{(\hat{x}_{\text{Sc}}^{\alpha'} - \hat{x}_{\text{Sc}}^\alpha)}{(\hat{x}_{\text{Mg}}^{\alpha'} - \hat{x}_{\text{Mg}}^\alpha)} = \frac{D_{\text{Sc}}}{D_{\text{Mg}}} \frac{(x_{\text{Sc}}^\alpha - x_{\text{Sc}}^\infty)}{(x_{\text{Mg}}^\alpha - x_{\text{Mg}}^\infty)}, \quad (5)$$

where  $\hat{x}_{\text{Sc}}^\alpha$ ,  $\hat{x}_{\text{Mg}}^\alpha$ ,  $\hat{x}_{\text{Sc}}^{\alpha'}$ , and  $\hat{x}_{\text{Mg}}^{\alpha'}$  denote mole fractions of Sc and Mg on the Al ( $\alpha$ ) and Al<sub>3</sub>Sc ( $\alpha'$ ) sides of the interface for a precipitate of radius  $R$ ,  $\gamma$  is the interfacial free energy, the variables  $\mu_i^\alpha$  and  $\mu_i^{\alpha'}$  correspond to bulk chemical potentials, and  $\bar{V}_i$  is the partial molar volume for species  $i$  in the precipitate ( $\alpha'$ ) phase. The variables  $x_{\text{Sc}}^\infty$  and  $x_{\text{Mg}}^\infty$  correspond to far-field solute concentrations in the matrix phase. The first three equations represented by Eq. (4) correspond to the well-known Gibbs–Thomson conditions incorporating the effect of capillarity in the formulation of the conditions for local thermodynamic equilibrium [26], while Eq. (5) reflects the constraint imposed by solute flux balance.

Since values for the chemical potentials in the ternary Al<sub>3</sub>Sc intermetallic phase, required in the solution of Eqs. (4) and (5), are unavailable from experimental measurements, we have employed first-principles free-energy models in calculations of the equilibrium phase compositions. The bulk free energies were derived within a model of non-interacting substitutional defects through a generalization of the approach outlined in [13,29–31]. Such a non-interacting defect model for the free energy is expected to be highly accurate for the dilute solute concentrations considered in the present study. In this approach to modeling

the thermodynamics of the bulk  $\alpha$ - and  $\alpha'$ -phases, the free-energy models take the following form:

$$F^\alpha = F_0^\alpha + k_{\text{B}} T x_{\text{Al}} \ln x_{\text{Al}} + x_{\text{Sc}} [\Delta F_{\text{Sc}}^\alpha + k_{\text{B}} T \ln x_{\text{Sc}}] + x_{\text{Mg}} [\Delta F_{\text{Mg}}^\alpha + k_{\text{B}} T \ln x_{\text{Mg}}], \quad (6)$$

$$F^{\alpha'} = F_0^{\alpha'} + \frac{3}{4} \left\{ k_{\text{B}} T x_{\text{Al}}^{\text{Al}} \ln x_{\text{Al}}^{\text{Al}} + x_{\text{Sc}}^{\text{Al}} [\Delta F_{\text{Sc}}^{\alpha',\text{Al}} + k_{\text{B}} T \ln x_{\text{Sc}}^{\text{Al}}] + x_{\text{Mg}}^{\text{Al}} [\Delta F_{\text{Mg}}^{\alpha',\text{Al}} + k_{\text{B}} T \ln x_{\text{Mg}}^{\text{Al}}] \right\} + \frac{1}{4} \left\{ k_{\text{B}} T x_{\text{Sc}}^{\text{Sc}} \ln x_{\text{Sc}}^{\text{Sc}} + x_{\text{Al}}^{\text{Sc}} [\Delta F_{\text{Al}}^{\alpha',\text{Sc}} + k_{\text{B}} T \ln x_{\text{Al}}^{\text{Sc}}] + x_{\text{Mg}}^{\text{Sc}} [\Delta F_{\text{Mg}}^{\alpha',\text{Sc}} + k_{\text{B}} T \ln x_{\text{Mg}}^{\text{Sc}}] \right\},$$

where in the  $\alpha$ -Al phase  $x_{\text{Al}}$ ,  $x_{\text{Sc}}$  and  $x_{\text{Mg}}$  are the mole fractions of Al, Sc and Mg, while in the  $\alpha'$ -Al<sub>3</sub>Sc phase  $x_{\text{Al}}^{\text{Al}}$  and  $x_{\text{Al}}^{\text{Sc}}$  denote Al mole fractions on the Al and Sc sublattices, respectively, and similarly for  $x_{\text{Sc}}^{\text{Al}}$ ,  $x_{\text{Sc}}^{\text{Sc}}$ ,  $x_{\text{Mg}}^{\text{Al}}$  and  $x_{\text{Mg}}^{\text{Sc}}$ . The quantities  $\Delta F_j^\alpha$  for the  $\alpha$ -Al phase in Eq. (6) denote the free energy to form a substitutional impurity of type  $j$  in pure Al; at zero temperature these are simply the heats of solution ( $\Delta E_j^\alpha$ ), while at finite temperature  $\Delta F_j^\alpha$  generally contains entropic contributions of vibrational and electronic origins. Similarly, for the  $\alpha'$ -Al<sub>3</sub>Sc phase  $\Delta F_j^{\alpha',k}$  denotes the free energy to form substitutional impurity  $j$  on sublattice  $k$ .

The various defect energies entering in Eq. (6) were computed from first-principles using the ab initio total-energy and molecular-dynamics program VASP (Vienna ab initio simulation package) developed at the Institut für Materialphysik of the Universität Wien [32–34]. In these calculations, use was made of ultrasoft pseudopotentials [35], the local-density approximation, and an expansion of the electronic wave functions in plane waves. Further details of the calculations can be found in [31]. Calculations of the point-defect energies entering Eq. (6) were performed employing 64-atom supercells, and were derived from the relation  $\Delta E_j^{\phi,k} = E_j^{\phi,k} - E^\phi + (E_k - E_j)$ , where  $E_j^{\phi,k}$  is the energy of the supercell of phase  $\phi$  containing an impurity of type  $j$  on site  $k$ ,  $E^\phi$  is the energy of the supercell for stoichiometric phase  $\phi$ , and  $E_j$  and  $E_k$  denote the energies per atom of pure species  $j$  and  $k$  in their respective equilibrium crystal structures, respectively.

The results of the supercell defect-energy calculations are presented in Fig. 7. It is seen that Sc is calculated to have a large and negative heat of solution in  $\alpha$ -Al, while the corresponding value for Mg is near zero. In the  $\alpha'$ -Al<sub>3</sub>Sc phase, all substitutional defects are seen to have relatively large and positive formation energies. The  $\Delta E$  values given in Fig. 7 were used in Eq. (6) to derive bulk chemical potentials, which formed the basis for the computation of the equilibrium concentrations given in Table 3. In these calculations we also included vibrational-entropy contributions to  $F_0^\alpha$ ,  $F_0^{\alpha'}$  and  $\Delta F_{\text{Sc}}^\alpha$ , since these contributions have been shown to be crucial for reproducing the measured binary Al–Al<sub>3</sub>Sc solvus boundary compositions [29]. The details of the vibrational-entropy calculations are given in [29,30].

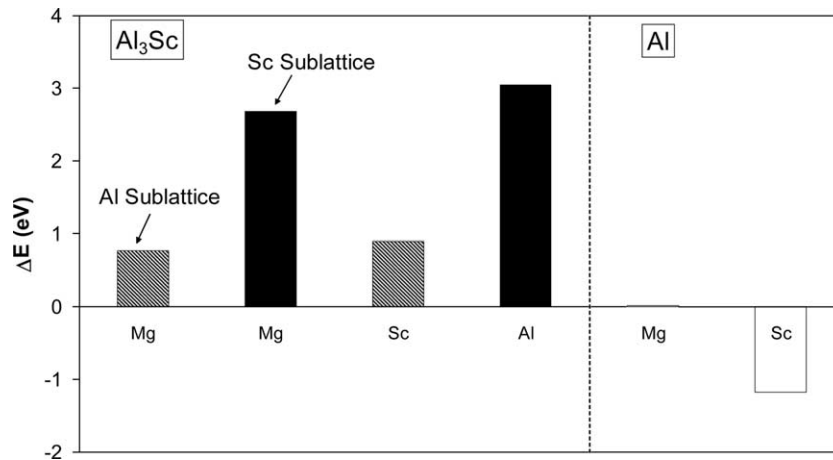


Fig. 7. Calculated substitutional point-defect energies in Al and Al<sub>3</sub>Sc phases. Results for  $\alpha$ -Al are plotted on the right and those for  $\alpha'$ -Al<sub>3</sub>Sc on the left. Solid and hatched bars denote defect energies on the Sc and Al sublattices in the  $\alpha'$ -Al<sub>3</sub>Sc phase, while the white bars denote heats of solution for Mg and Sc in  $\alpha$ -Al.

Table 3 lists values of the interface concentrations calculated from Eqs. (4) and (5) for precipitates of radii 2 and 4 nm at an aging temperature of 300 °C. For comparison we also list compositions corresponding to two-phase equilibrium between bulk ( $R \rightarrow \infty$ )  $\alpha$  and  $\alpha'$ -phases in a ternary alloy with the composition Al–2.2 at.% Mg–0.12 at.% Sc considered experimentally. For this alloy composition, the bulk equilibrium compositions derived from first-principles (final row of Table 3) are in very reasonable agreement with the values of  $\hat{x}_{\text{Sc}}^{\alpha} = 7.2 \times 10^{-4}$  at.% and  $\hat{x}_{\text{Mg}}^{\alpha} = 2.2$  at.%, derived independently by Murray [36] from empirical free-energy models.

In our calculations of the interface compositions listed in Table 3, values for the far-field matrix compositions in Eq. (5) were taken as  $x_{\text{Sc}}^{\infty} = 0.014 \pm 0.001$  at.% and  $x_{\text{Mg}}^{\infty} = 2.35 \pm 0.02$  at.%, as measured by APT in alloys aged for 1040 h [8]. We further made use of the following measured values for the solute diffusivities in Al:  $D_{\text{Sc}} = 8.84 \times 10^{-20} \text{ m}^2 \text{ s}^{-1}$  and  $D_{\text{Mg}} = 1.62 \times 10^{-16} \text{ m}^2 \text{ s}^{-1}$  [17,32]. Additionally, we employed a value for  $\gamma$  equal to  $0.175 \text{ J m}^{-2}$ , as derived from first-principles calculations for planar interfaces between pure Al and stoichiometric Al<sub>3</sub>Sc [21] ( $\gamma$  is assumed to be constant and independent of composition).

A comparison of the results in the first two rows of Table 3 with those corresponding to bulk phases (final row) shows that the effects of capillarity and solute flux balance are estimated to give rise to relatively small ( $\sim 10\%$ ) changes in the matrix Mg concentration at the growing precipitate/matrix interface. Thus, the pronounced interfacial enhancement of Mg measured by APT cannot be interpreted simply as reflecting the effects of capillarity and solute flux balance in a model of diffusion-limited precipitate growth. Additional first-principles calculations, discussed in the following section, suggest instead that the observed interfacial segregation of Mg reflects an equilibrium segregation effect, arising from electronic interactions between Sc and Mg atoms in Al.

#### 4.2.2. Equilibrium segregation energies for Mg at a coherent Al/Al<sub>3</sub>Sc interface

First-principles VASP calculations were conducted to investigate the energetics of Mg solute atoms in the vicinity of planar coherent Al/Al<sub>3</sub>Sc interfaces aligned parallel to {200} crystallographic planes. The heats of solution for Mg solute atoms were computed as a function of distance in the vicinity of a planar Al/Al<sub>3</sub>Sc interface employing supercell geometries with periodic boundary conditions. Preliminary results from these calculations were reported in [12] and further details were given in [13]. The supercells used in these calculations contained periodic vectors in the plane of the interface ( $\mathbf{a}_1$  and  $\mathbf{a}_2$ ) with lengths four times the face-centered cubic (fcc) nearest-neighbor spacing:  $\mathbf{a}_1 = a(2, -2, 0)$ ,  $\mathbf{a}_2 = a(2, 2, 0)$ , where  $a$  is the fcc lattice constant. In the  $z$ -direction, normal to the interface, the periodic length corresponded to 14 fcc unit cell dimensions. The total number of atoms in these supercells was 412. The results presented below were derived using a value for the in-plane lattice constant ( $a$ ) equal to that for the bulk Al<sub>3</sub>Sc phase; the dimension of the supercell in the  $z$ -direction was then adjusted to give zero total  $zz$ -stress for a pure Al/Al<sub>3</sub>Sc interface (without Mg additions). Additional calculations were performed using a value of the in-plane lattice constant equal to that for bulk fcc Al, and only minor differences in the calculated segregation energies were obtained. In this section we report the solution energy of a single Mg atom placed at various crystal sites in the vicinity of the Al/Al<sub>3</sub>Sc (002) interface. For calculations in which Mg substitutes on the Al side of the interface, the supercells contained a total of nine unit cells of fcc Al and five unit cells of Al<sub>3</sub>Sc. Similarly, for calculations of Mg impurity formation energies on the Al<sub>3</sub>Sc side of the interface we employed supercells with five fcc-Al unit cells and nine Al<sub>3</sub>Sc unit cells. Magnesium impurity formation energies were derived for substitution both on Al and Sc sites in the supercell; in all cases the formation energies on Sc lattice positions were sufficiently high to yield negligible equilibrium Mg concentrations on these sites.

In Fig. 8 we plot the formation energies ( $\Delta E$ ) for substituting Mg for Al as a function of distance across the coherent (002) Al/Al<sub>3</sub>Sc planar interface. The values of  $\Delta E$  calculated on the Al<sub>3</sub>Sc side of the interface are roughly 0.6 eV larger than in pure Al, indicative of the strong energetic preference for the partitioning of Mg to the matrix phase. In terms of the APT measurements, the most important feature of the results shown in Fig. 8 is the significantly negative formation energy calculated on the Al side of the interface at the crystallographic site corresponding to a second neighbor of the interface Sc atoms (the site labeled “1” in Fig. 8). The value of  $\Delta E$  at this site is computed to be  $\sim 0.1$  eV lower than the heat of solution for Mg atoms in bulk Al. This segregation energy ( $\Delta E$ ) thus provides a reasonably strong driving force for the equilibrium segregation of Mg atoms to the (002) coherent Al/Al<sub>3</sub>Sc interface.

To make explicit contact with the experimental results, the energies derived from the first-principles calculations have been used within a mean-field (Bragg–Williams) model for the configurational free energy (similar to Eq. (6)) to compute the equilibrium solute composition profiles across a planar Al/Al<sub>3</sub>Sc {200} interface at 300 °C. Within this approximation, the equilibrium concentration of Mg atoms at site  $j$ ,  $x_{\text{Mg}}(j)$ , is given as  $x_{\text{Mg}}(j) = x_{\text{Mg}}^0 \exp\{-[\Delta E(j) - \Delta E(\infty)]/k_{\text{B}}T\}$ , where  $x_{\text{Mg}}^0$  is the bulk Mg concentration in  $\alpha$ -Al,  $\Delta E(j)$  is the formation energy of a substitutional Mg impurity at site  $j$  near the interface, and  $\Delta E(\infty)$  is the heat of solution in bulk  $\alpha$ -Al (far from the interface). The calculated Mg concentration profile is shown in Fig. 9, and was derived assuming a bulk Mg concentration in Al of  $\Delta E(\infty) = 2.4$  at.%. The plot features a five- to sixfold enhancement of the  $x_{\text{Mg}}$  in the plane positioned one lattice constant from the interface Sc atoms. In comparison to the

APT results for Mg plotted in Fig. 5, the calculated concentration profile is considerably narrower with a larger value for the Mg enhancement factor. These differences between the experimental and theoretically calculated composition profiles may be due to the effects discussed in Section 4.1 associated with the APT technique. Specifically, the measured width of the concentration profile at the Al/Al<sub>3</sub>Sc interface is probably greater than the real width due to effects associated with the field-evaporation process [24], which make a concentration profile appear broader than it is (see Section 4.1).

Due to these differences in the width, a more meaningful comparison between experiment and theory can be made in terms of the integrated area under the Mg concentration profiles. Specifically, the relative Gibbsian interfacial adsorption segregation of Mg with respect to Al and Sc provides a quantitative thermodynamic description of the degree of equilibrium Mg segregation. If we interpret the Mg segregation to reflect an equilibrium segregation effect, we can estimate the values of the Gibbsian excess quantities for Al (negative value), Mg and Sc (both positive values) as the areas under the concentration curves in the proximity histogram as displayed in Fig. 5 [29]. The value thus derived from the experimental data is  $\Gamma_{\text{Mg}}^{\text{rel}} = 1.9 \pm 0.5$  atom nm<sup>-2</sup>, which is found to be independent of aging time after 0.5 h at 300 °C. By comparison,  $\Gamma_{\text{Mg}}^{\text{rel}}$  derived from the calculated composition profiles is  $\sim 1.2$  atom nm<sup>-2</sup>. Thus, experiments and calculations yield values for the relative Gibbsian interfacial excess of Mg, which are approximately the same within the experimental uncertainty of  $\pm 0.5$  atom nm<sup>-2</sup>. The good level of agreement between experiment and theory thus supports strongly the conclusion that the measured interfacial enhancement of Mg reflects a pronounced

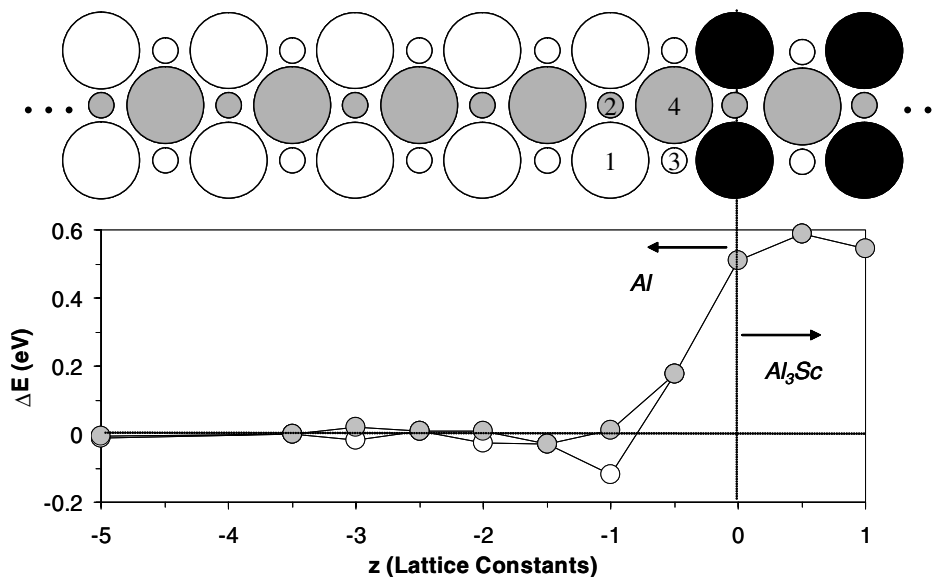


Fig. 8. Calculated formation energies for substitution of Mg for Al as a function of distance from the (0 0 2)  $\alpha$ -Al/Al<sub>3</sub>Sc interface. A projection of the interface atomic structure of the interfacial region is shown on top, with white and gray circles denote Al positions in planes parallel to the interface, and black circles corresponding to Sc sites. In this projection the large circles denote atomic sites positioned 0.5 of a lattice constant below those indicated by the smaller circles. The formation energies are plotted as a function of distance normal to the interface in the lower plot; white and gray circles denote values of  $\Delta E$  derived for the corresponding sites in each plane shown in the projection above.

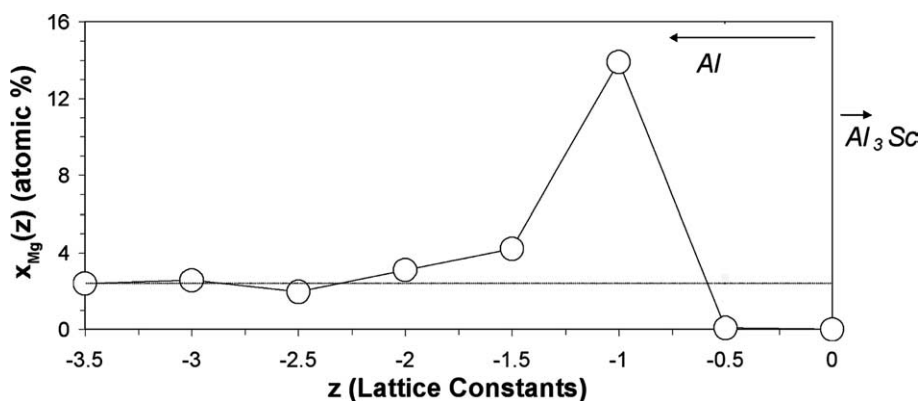


Fig. 9. Calculated Mg concentration profile near the  $\alpha$ -Al/Al<sub>3</sub>Sc interface. Compositions have been derived from the results in Fig. 8 assuming a bulk Mg concentration in the Al phase of 2.4 atomic %.

equilibrium effect associated with the segregation of this species to planar coherent Al/Al<sub>3</sub>Sc heterophase interfaces.

It is noteworthy that the calculated segregation energy derived from the first-principles supercell calculations are found to be highly insensitive to the imposed value of the in-plane lattice parameter (the value of which was varied in the calculations between the equilibrium lattice constants for pure Al and Al<sub>3</sub>Sc phases as described above). Furthermore, the calculated segregation energy is found to change by less than 10% if the interface positions are fixed at ideal fcc positions. That is, the calculated segregation energy is found to be insensitive to the state of strain at the interface. Thus the origin of the calculated segregation energy appears not to originate from elastic strain energy. Rather, we interpret the result as being a manifestation of the nature of Mg–Sc electronic interactions in an Al-rich alloy.

In support of this interpretation we have computed the solute interaction energies up to fourth neighbor distances for Mg–Mg, Sc–Sc and Mg–Sc pairs in pure Al employing VASP and 216-atom supercells ( $6 \times 6 \times 6$  primitive fcc unit cells). The results are shown in Fig. 10. Strong and relatively long-ranged interactions are derived for both Mg–Sc and Sc–Sc pairs. The magnitude and oscillating nature of the Sc–Sc results are consistent with theoretical models for transition-metal interactions in Al due to Carlsson and Moriarty [38,39]. For both Sc–Sc and Mg–Sc we obtain repulsive interactions at first and third neighbors, and attractive interactions at second and fourth. The magnitude and spatial variation of these interactions were found to be primarily electronic in origin; very similar values to those plotted in Fig. 10 were obtained in supercell calculations where the atoms were constrained to their bulk fcc lattice sites (i.e., removing any elastically induced contribution to the interactions). In light of the results in Fig. 10, the overall magnitude of the calculated segregation energy, as well as the preferred binding site for Mg at the Al/Al<sub>3</sub>Sc {200} heterophase interface, can be rationalized as follows.

The supercell calculations yield a preferred binding site for Mg, labeled “1” in Fig. 8, that contains the maximum

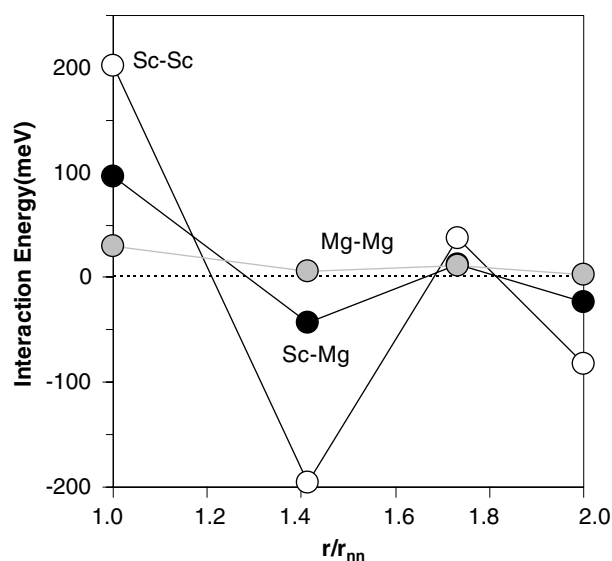


Fig. 10. Mg–Mg, Mg–Sc and Sc–Sc interaction energies in an Al host, calculated as a function of separation  $r$  normalized by the nearest-neighbor distance ( $r_{\text{NN}}$ ).

number of both second neighbors (one per Mg atom) and fourth neighbors (four per Mg atom) to interface Sc atoms, while featuring no nearest or third-nearest neighbor repulsive Mg–Sc pairs. Assuming that the alloy energetics are dominated by pair interactions, the interaction energies plotted in Fig. 10 can be used to derive a magnitude for the Mg binding energy at site “1” equal to 0.14 eV. This result is in very good overall agreement with the value derived from direct supercell calculations (see Fig. 8). Furthermore, the Mg impurity energy at the site labeled “2” in Fig. 8 is computed to be near zero in the direct supercell calculations. This result is again consistent with a bond-counting analysis considering that this site features only third neighbor interactions with interface Sc atoms; the magnitude of the third-neighbor Mg–Sc interactions are shown to be relatively small in Fig. 10. Finally, both sites “3” and “4” in Fig. 8 are calculated to have relatively large positive Mg impurity formation energies on the order of 0.2 eV. This result is again consistent with bond

counting, given the fact that these sites have two nearest-neighbor bonds with interface-Sc atoms, each contributing approximately 0.1 eV of interaction energy to  $\Delta E$  according to Fig. 10. Overall, the very good agreement between the directly calculated formation energies at the interface sites, and the corresponding values derived from a relatively simple bond-counting analysis, suggests strongly that Mg segregation at the Al/Al<sub>3</sub>Sc interface can be interpreted as being a reflection of strong Mg–Sc electronic interactions in Al.

The type of bond-counting analysis described in the previous paragraph provides a convenient framework for analyzing the magnitude of the anisotropy associated with Mg segregation to a coherent Al/Al<sub>3</sub>Sc interface. Such an analysis is interesting in light of the experimental observations by Marquis et al. [8,14] showing that Mg additions to Al–Sc lead to a pronounced change in the morphology of Al<sub>3</sub>Sc precipitates from highly faceted (with well-developed {100}, {110} and {111} facets) to a spheroidal morphology. Due to the higher areal densities of sites containing attractive second and fourth neighbor interactions with interface Sc atoms, Mg segregation is estimated to be roughly a factor of three and 2.5 larger for {110} and {111} interfaces, respectively, relative to the lower-energy {100} orientation. We consider the analysis for {100} versus {110} orientations in detail in Fig. 11. This figure highlights with gray and hatched circles the atomic sites that are predicted to have appreciable binding energies for Mg. In the case of {100} discussed, there is one attractive site per area  $a^2$ , with a segregation energy of approximately 0.1 eV. By comparison, the {110} interface contains two attractive sites per area,  $\sqrt{2}a^2$ . The site colored gray in Fig. 11 contains two second-nearest-neighbor and five fourth-neighbor Sc atoms. From the interaction energies in Fig. 10, this site is thus predicted to have a binding energy of approximately –0.2 eV, leading to a site concentration at 300 °C that is predicted to be nearly pure Mg (assuming a bulk composition of 2.4 at.% and using a Bragg–Williams model as above). The second binding site

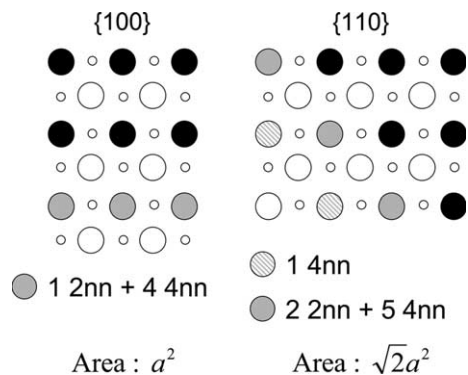


Fig. 11. The projections compare the atomic geometries near {100} and {110} interfaces. As in Fig. 8, small and large circles denote atomic sites separated by 0.5 of a lattice spacing in the direction out of the page. Black and white circles denote Sc and Al sites, respectively. The solid and hatched gray circles denote Al sites near the interface displaying attractive binding energies for Mg, as described in the text.

for a {110} interface, indicated by the hatched circle in Fig. 11, shares one fourth neighbor with interface-Sc atoms and thus has a relatively small binding energy of roughly –0.025 eV, leading to a concentration enhancement of about 1.7 times the bulk concentration at 300 °C. The net result is an enhancement of  $\Gamma_{\text{Mg}}^{\text{rel}}$  by approximately a factor of three for a {110} interface relative to {100}. A similar analysis leads to the prediction of a value for  $\Gamma_{\text{Mg}}^{\text{rel}}$  for {111} orientations that is enhanced by approximately a factor of two relative to {100}.

Using the Gibbs adsorption theorem, Mg segregation is predicted to lower the free energy of {100}, {111} and {110} interfaces by approximately 10, 20 and 30 mJ m<sup>–2</sup>, respectively. Magnesium segregation thus lowers the free energy of {110} and {111} orientations by 10–20 mJ m<sup>–2</sup> relative to {100} orientations. In [13], calculated interfacial free energies for Al/Al<sub>3</sub>Sc interfaces in binary Al–Sc showed a {100} vs. {111} anisotropy of 25 mJ m<sup>–2</sup> at 300 °C (with the free energy of {110} estimated to be similar to {111}). The present results thus suggest that Mg segregation leads to a substantial reduction in the anisotropy of the Al/Al<sub>3</sub>Sc interfacial free energies, consistent with the observed reduction in precipitate faceting induced by the addition of Mg [8,13] and the resulting spheroidal morphology.

#### 4.3. Heterogeneous nucleation of Al<sub>3</sub>Sc precipitates?

As the aging time increases from 2 to 1040 h, the Mg segregation peak observed at early time splits into two peaks, one at the interface separated from a peak at the center of the precipitates (Fig. 6). In particular after 1040 h aging, 15–42 Mg atoms were detected at the center of the Al<sub>3</sub>Sc precipitates. It is speculated that Al<sub>3</sub>Sc precipitation occurs as a result of interactions between Mg and Sc atoms with vacancies, which leads to a faster nucleation rate than in the binary Al–Sc alloy, as demonstrated by the microhardness measurements [5]. Indeed, from an analysis of the early stages of decomposition, the experimental number of Mg–Sc dimers in the reconstruction is somewhat greater than the expected number of pairs in the case of a perfectly random solid-solution. The experimental number of Mg–Sc dimers defined by a maximum separation distance between the Mg and Sc atoms of 0.5 nm, is 1082 for a total number of ions,  $N$ , equal to  $1.154 \times 10^6$ ; this yields a concentration of Mg–Sc dimers equal to 0.0937 at.%. The theoretical concentration of dimers (first nearest and second nearest-neighbors),  $x_{\text{Mg-Sc}}$ , defined by the number of dimers divided by the total number of atoms, is given by:

$$x_{\text{Mg-Sc}} = 18x_{\text{Mg}}x_{\text{Sc}} \exp\left(\frac{g_{\text{Mg-Sc}}^b}{k_{\text{B}}T}\right), \quad (7)$$

where  $x_{\text{Mg}}$  and  $x_{\text{Sc}}$  are the average concentrations of Mg and Sc atoms, and  $g_{\text{Mg-Sc}}^b$  is an average Gibbs binding free energy between Mg and Sc atoms for first and second nearest-neighbors. In the case of a random solid solution, the binding energy is zero therefore leading to an expected

number of first and second nearest-neighbor dimers, given by  $18x_{\text{Mg}}x_{\text{Sc}} = 0.0693$  at.%, The measured concentration of dimers is 60% of the actual value, assuming an ion detection efficiency of 60%. An estimate of the average Gibbs binding free energy in the as-quenched state is then calculated to be 0.040 eV. After 20 min aging, the measured concentration of dimers is 0.0617 at.%, compared to the random solution concentration of 0.0484 at.%, which yields an average binding energy of 0.037 eV. A positive value of  $g_{\text{Mg-Sc}}^{\text{b}}$  indicates an attractive interaction between atoms, in agreement with the first principles calculations in Fig. 10.  $\text{Al}_3\text{Sc}$  precipitation occurs as a result of interactions between Mg and Sc atoms with vacancies, which leads to a faster nucleation rate than in the binary Al–Sc alloy. The high concentration of quenched-in vacancies and their high mobility, even at room-temperature, could explain a fairly high number density of Mg–Sc dimers and, during the formation of a stable nucleus involving the Mg–Sc dimers, Mg atoms may get trapped within the nanoscale growing  $\text{Al}_3\text{Sc}$  precipitates, as Sc diffuses to the precipitates.

We were unable to find diffusion data for any element in  $\text{Al}_3\text{Sc}$  in the literature. The presence of a Mg-rich  $\text{Al}_3\text{Sc}$  precipitate core after a long aging time, i.e. 1040 h, (Fig. 7) indicates, however, a very small diffusivity of Mg in the  $\text{Al}_3\text{Sc}$  phase. An estimate of the diffusivity of Mg in  $\text{Al}_3\text{Sc}$  at 300 °C is obtained using  $\sqrt{\langle d^2 \rangle} = \sqrt{6D_{\text{Mg}}^{\text{Al}_3\text{Sc}}t}$ , where  $d$  is the precipitate diameter and the factor of six is from three-dimensional diffusion. The estimated diffusivity is therefore given by:

$$D_{\text{Mg}}^{\text{Al}_3\text{Sc}} \cong \frac{\langle d^2 \rangle}{6t}. \quad (8)$$

For  $t = 1040$  h, Eq. (8) yields a value of  $2 \times 10^{-23} \text{ m}^2 \text{ s}^{-1}$ , which is approximately seven orders of magnitude smaller than the diffusivity of Mg in Al at 300 °C ( $1.62 \times 10^{-16} \text{ m}^2 \text{ s}^{-1}$ ) [37]. This indicates that it is difficult for Mg to diffuse through the  $\text{Al}_3\text{Sc}$  phase to the matrix, which explains the shape of the Mg concentration profiles observed in Figs. 6 and 7, even though the equilibrium ternary Al–Mg–Sc phase diagram [36] does not predict any Mg solubility in the  $\text{Al}_3\text{Sc}$  phase. And the first principles calculations presented in Section 4.2 also indicate essentially no solubility of Mg in  $\text{Al}_3\text{Sc}$ .

## 5. Conclusions

- Magnesium segregation occurring at the perfectly coherent  $\alpha\text{-Al}/\text{Al}_3\text{Sc}$  heterophase interface was studied experimentally using atom-probe tomography (APT) for an Al–2.2 Mg–0.12 at.% Sc alloy aged at 300 °C.
- The thermodynamic equilibrium Mg segregation behavior corresponds to a measured relative Gibbsian excess of Mg with respect to Al and Sc of  $1.9 \pm 0.5$  atoms  $\text{nm}^{-2}$ .

- In addition to the Mg segregation at perfectly coherent  $\alpha\text{-Al}/\text{Al}_3\text{Sc}$  heterophase interfaces we also detected Mg at the centers of  $\text{Al}_3\text{Sc}$  precipitates, Fig. 7, which is kinetically trapped since Mg is insoluble in  $\text{Al}_3\text{Sc}$ . The diffusivity of Mg in  $\text{Al}_3\text{Sc}$  is estimated to be  $2 \times 10^{-23} \text{ m}^2 \text{ s}^{-1}$ , which is approximately seven orders of magnitude smaller than the diffusivity of Mg in Al at 300 °C ( $1.62 \times 10^{-16} \text{ m}^2 \text{ s}^{-1}$ ).
- The effects of capillarity and solute flux balance are theoretically estimated to give rise to relatively small ( $\sim 10\%$ ) changes in the matrix Mg concentration at the growing coherent  $\alpha\text{-Al}/\text{Al}_3\text{Sc}$  heterophase interface. Therefore, the pronounced interfacial enhancement of Mg measured by APT cannot be interpreted simply as reflecting the effects of capillarity and solute flux balance in a model of diffusion-limited precipitate growth.
- The segregation of Mg at the coherent  $\alpha\text{-Al}/\text{Al}_3\text{Sc}$  heterophase interface was studied theoretically employing ab initio calculations. These calculations demonstrate that the driving force for segregation of Mg is due to electronic interactions rather than elastic strain relaxation associated with highly over-sized Mg atoms. The calculated value of the relative Gibbsian excess of Mg with respect to Al and Sc is ca. 1.2 atoms  $\text{nm}^{-2}$ , which is in good agreement with the experimental value.
- The results of the supercell defect-energy calculations are presented in Fig. 8. It is seen that Sc is calculated to have a large and negative heat of solution in  $\alpha\text{-Al}$ , while the corresponding value for Mg is near zero. In the  $\alpha'\text{-Al}_3\text{Sc}$  phase, all substitutional point defects are seen to have relatively large and positive formation energies.
- We have computed the solute interaction energies up to fourth neighbor distances for Mg–Mg, Sc–Sc and Mg–Sc pairs in pure Al employing VASP and 216-atom supercells ( $6 \times 6 \times 6$  primitive fcc unit cells), see results in Fig. 11. Strong and relatively long-ranged interactions are derived for both Mg–Sc and Sc–Sc pairs. The magnitude and oscillating nature of the Sc–Sc results are consistent with theoretical models for transition-metal interactions in Al.
- Using the Gibbs adsorption theorem, Mg segregation is predicted to lower the free energy of  $\{100\}$ ,  $\{111\}$  and  $\{110\}$  heterophase interfaces by roughly 10, 20 and 30  $\text{mJ m}^{-2}$ , respectively. Magnesium segregation thus lowers the free energy of  $\{110\}$  and  $\{111\}$  orientations by 10–20  $\text{mJ m}^{-2}$  relative to  $\{100\}$  orientations.
- These present theoretical results suggest that Mg segregation leads to a substantial reduction in the anisotropy of the  $\alpha\text{-Al}/\text{Al}_3\text{Sc}$  interfacial free energies, which is consistent with our HREM observations of a reduction in precipitate faceting induced by the addition of Mg to Al–Sc alloys [8].

## Acknowledgments

This research is supported by the United States Department of Energy, Basic Sciences Division, under contracts

DE-FG02-98ER45721 (EAM and DNS) and DE-FG02-01ER45910 (MDA) and the Air Force Research Laboratory, the Air Force Office of Scientific Research under contract F33615-01-C-5214 (CW). The authors thank Professors P.W. Voorhees and D.C. Dunand for very interesting discussions, Dr. D. Isheim for help in using an atom-probe tomograph, and Alcoa Inc. and Ashurst Inc. for supplying the Al–Sc master alloy. The calculations performed in this work made use of resources at the National Energy Research Scientific Computing Center under Contract No. DE-AC03-76SF00098, and the DOD High Performance Computer Modernization Program at the Aeronautical Systems Center-Major Shared Resource Center on the IBM-SP3.

## References

- [1] Toporova LS, Eskin DG, Kharakterova ML, Dobatkina TB. Advanced aluminum alloys containing scandium. Amsterdam: Gordon & Breach; 1998.
- [2] Royset J, Ryum N. *Int Mater Rev* 2005;50:2.
- [3] Fuller CB, Murrey JL, Seidman DN. *Acta Mater* 2005;53:5401; Fuller CB, Seidman DN. *Acta Mater* 2005;53:5415.
- [4] van Dalen ME, Dunand DC, Seidman DN. *MS&T 2003 – Affordable metal matrix composites for high performance applications II*. Pittsburgh, PA: TMS; 2003. p. 195.
- [5] Marquis EA, Seidman DN, Dunand DC. *Acta Mater* 2003;51:4751.
- [6] Marquis EA. Ph.D. thesis, Northwestern University, 2002.
- [7] Marquis EA, Seidman DN. *Acta Mater* 2001;49:1909.
- [8] Marquis EA, Seidman DN. *Acta Mater* 2005;53:4259.
- [9] Marquis EA, Dunand DC. *Scripta Mater* 2002;47:503.
- [10] Fuller CB, Seidman DN, Dunand DC. *Acta Mater* 2003;4803:51.
- [11] King HW. *J Mater Sci* 1966;1:79.
- [12] Asta M, Ozolins V, Woodward C. *JOM* 2001;53(9):16.
- [13] Marquis EA, Seidman DN, Asta M, Woodward C, Ozolins V. *Phys Rev Lett* 2003;91:036101.
- [14] Hellman OC, Vandenbroucke J, Blatz du Rivage J, Seidman DN. *Mater Sci Eng A* 2001;327:29.
- [15] Miller MK, Smith GDW. *Atom probe microanalysis*. Pittsburgh: MRS; 1989.
- [16] Hellman OC, Vandenbroucke JA, Rüsing J, Isheim D, Seidman DN. *Microsc Microanal* 2000;6:437.
- [17] Rothman SJ, Peterson NL, Nowicki LJ, Robinson LC. *Phys Status Solidi B* 1974;63:K29.
- [18] Dregia SA, Wynblatt P. *Acta Metall Mater* 1991;39:771.
- [19] Krakauer BW, Seidman DN. *Phys Rev B* 1993;48:6724.
- [20] Lupis CHP. *Chemical thermodynamics of materials*. Englewood Cliffs, NJ: Prentice Hall; 1983.
- [21] Asta M, Foiles SM, Quong AA. *Phys Rev B* 1998;57:11265.
- [22] Isheim D, Csencsits R, Seidman DN. *Mater Res Soc Symp Proc* 2001;652:Y1021.
- [23] Isheim D, Seidman DN. *Mater Metall Trans A* 2002;33:2317.
- [24] Vurpillot F, Bostel A, Blavette D. *Appl Phys Lett* 2000;76:3127.
- [25] Kuehman CJ, Voorhees PW. *Metall Trans A* 1996;27:937.
- [26] The precipitates considered in this work are coherent, and the bulk  $\alpha$  and  $\alpha'$  phases are known to have a lattice parameter mismatch of roughly 0.6% in the ternary Al–Sc–Mg alloy at the aging temperature of 300 °C. As a consequence, the equations governing thermodynamic equilibrium, Eq. (1), should generally be modified to account for the elastic energy associated with coherency strains (e.g., [27]). For the precipitate radii relevant to the Al–Sc–Mg system (2–4 nm), the elastic energy density derived from Eshelby's model [28] of a spherical misfitting inclusion is found to be more than an order of magnitude smaller than the capillarity term  $2\gamma/R$ . We have therefore neglected detailed consideration of the effects associated with coherency strains in the analyses of interface solute concentrations.
- [27] Larché FC, Cahn JW. *Acta Metall* 1978;53:26.
- [28] Eshelby JD. *Proc Roy Soc London Ser A* 1957;241:376.
- [29] Ozolins V, Asta M. *Phys Rev Lett* 2001;86:448.
- [30] Asta M, Ozolins V. *Phys Rev B* 2001;64:094104.
- [31] Woodward C, Asta M, Kresse G, Hafner J. *Phys Rev B* 2001;63:094103.
- [32] Kresse G, Hafner J. *Phys Rev B* 1993;47:558.
- [33] Kresse G, Hafner J. *Phys Rev B* 1994;49:14251.
- [34] Kresse G, Furthmuller J. *Computat Mater Sci* 1996;6:15.
- [35] Kresse G, Furthmuller J. *Phys Rev B* 1996;54:11169.
- [36] Murray JL, private communication.
- [37] Fujikawa SI. *Defect Diff Forum* 1997;143–147:115.
- [38] Zou J, Carlsson AE. *Phys Rev B* 1993;47:2961.
- [39] Moriarty JA, Widom M. *Phys Rev B* 1997;56:7905.